

## Transition Strength Measurements to Guide Magic Wavelength Selection in Optically Trapped Molecules

K. H. Leung,<sup>1</sup> I. Majewska,<sup>2</sup> H. Bekker,<sup>1,\*</sup> C.-H. Lee,<sup>1,†</sup> E. Tiberi,<sup>1</sup> S. S. Kondov,<sup>1,‡</sup> R. Moszynski,<sup>2</sup> and T. Zelevinsky<sup>1,§</sup>

<sup>1</sup>*Department of Physics, Columbia University, 538 West 120th Street, New York, New York 10027-5255, USA*

<sup>2</sup>*Quantum Chemistry Laboratory, Department of Chemistry, University of Warsaw, Pasteura 1, 02-093 Warsaw, Poland*



(Received 23 May 2020; accepted 7 September 2020; published 9 October 2020)

Optical trapping of molecules with long coherence times is crucial for many protocols in quantum information and metrology. However, the factors that limit the lifetimes of the trapped molecules remain elusive and require improved understanding of the underlying molecular structure. Here we show that measurements of vibronic line strengths in weakly and deeply bound  $^{88}\text{Sr}_2$  molecules, combined with *ab initio* calculations, allow for unambiguous identification of vibrational quantum numbers. This, in turn, enables the construction of refined excited potential energy curves, informing the selection of magic wavelengths that facilitate long vibrational coherence. We demonstrate Rabi oscillations between far-separated vibrational states that persist for nearly 100 ms.

DOI: 10.1103/PhysRevLett.125.153001

The interplay of light and matter has enabled major strides in creating and controlling ultracold atoms and molecules. Exquisite control over the dense internal structure of molecules, in particular, offers promising avenues for tests of fundamental physics [1–6], cold controlled chemistry and collisions [7–12], quantum simulation [13–15], quantum computation [16–19], and compact terahertz frequency references [20]. Addressing the internal states with high fidelity necessitates the manipulation of spatial and motional degrees of freedom. For cold neutral gases, one common approach is the use of optical traps. Given two molecular states, the differential trap-induced light shifts and motional decoherence can be eliminated by tuning the frequency of the trap light close to a narrow rovibronic transition such that the dynamic polarizabilities are equal. Such magic wavelength traps were recently demonstrated to extend the vibrational [21] and rotational [22,23] coherence times of an ensemble of ultracold molecules. As with atomic lattice clocks [24,25], scattering of lattice laser light is expected to play a central role in limiting achievable interrogation times. Accurate knowledge of the molecular structure is thus a primary step in the identification of specific loss channels involved in the interaction of the molecules and the trap light. Additionally, this knowledge will help determine feasible pathways for quantum state preparation of the molecules [26–29].

In this Letter, we employ Lamb-Dicke spectroscopy in an optical lattice and state-of-the-art *ab initio* calculations to measure and predict vibronic line strengths (or transition strengths) in  $^{88}\text{Sr}_2$  molecules spanning over 3 orders of magnitude. This is achieved by measuring light shifts induced by a coupling laser as it is swept across a transition of interest, resulting in avoided crossing curves from which the line strengths are extracted with minimal modeling.

Taken together with lattice sideband spectroscopy, these curves additionally furnish an accurate frequency-only measurement of molecular polarizability ratios. We focus on transitions between the electronic ground potential  $X^1\Sigma_g^+$  (henceforth referred to as  $X$ ) and singly excited Hund's case ( $c$ ) potentials  $(1)0_u^+$  and  $(1)1_u$  corresponding to the  $^1S_0$ - $^3P_1$  dissociation limit. By addressing both weakly and deeply bound states, the molecular potential energy curves are probed over a wide range of internuclear distances. We combine our measurements with spectroscopic data to construct refined potential curves for  $0_u^+$  and  $1_u$  in the Morse/Long-range form and apply the results to judiciously select magic wavelengths that alleviate the impact of both frequency instability and scattering of the lattice laser on coherent molecule-light interactions. We demonstrate a superposition of far-separated vibrational states that remains coherent for a record time of nearly 100 ms.

In the Born-Oppenheimer approximation, the wave function of a diatomic molecule is a product of its electronic and rovibrational parts. The rovibrational part  $|\chi_{n,\Omega}^{v,J}(R)\rangle$  is a function of the internuclear distance  $R$  and is labeled by the following quantum numbers: the electronic channel  $n$ , the vibrational number  $v$ , the total angular momentum  $J$ , and its projection onto the internuclear axis in the molecule-fixed frame  $\Omega$ . Following Ref. [30], the line strength for an electric-dipole transition between the rovibrational states described by the wave functions  $|\chi_{n,\Omega}^{v,J}(R)\rangle$  and  $|\chi_{n',\Omega'}^{v',J'}(R)\rangle$  is given by

$$S \equiv |H_{J'M'\Omega'}^{JM\Omega} \langle \chi_{n',\Omega'}^{v',J'}(R) | d_{\Omega'-\Omega}(R) | \chi_{n,\Omega}^{v,J}(R) \rangle|^2, \quad (1)$$

where  $d_{\Omega'-\Omega}(R)$  is the electronic transition dipole moment,  $M$  is the projection of the total angular momentum onto the

lab-frame  $Z$  axis, and  $H_{J'M'\Omega'}^{JM\Omega}$  is the rotational factor defined in the Supplemental Material [31]. In the case of transitions driven by linearly polarized light along the quantization axis, the selection rules force  $M' = M$ . Equation (1) can easily be generalized to the multichannel case by introducing a sum over  $n, n', \Omega$ , and  $\Omega'$  before taking the absolute square. The quantity of interest that is readily accessible is the Rabi frequency

$$f_R = \frac{1}{\hbar} \sqrt{\frac{2IS}{\epsilon_0 c}}, \quad (2)$$

which quantifies the strength of coupling between two states when driven by a laser with intensity  $I$ , leading to observable light shifts in the molecular spectra. In this study, we measure the light shifts induced either by the optical lattice, which also acts as the trap as in Fig. 1(a), or by an anti-Stokes laser as in Fig. 1(b).

In the scheme shown in Fig. 1(a), we explore the coupling of  $X(v=6, J=0)$  to a set of  $J'=1$  resonances near the bottom of the  $1_u$  potential well by the optical lattice. For a given lattice detuning  $\Delta$  from the  $1_u$  state and the corresponding Rabi frequency  $f_R$ , the additional light shift on  $X(6, 0)$  is  $f_R^2/4\Delta$  in the limit  $\Delta \gg f_R$ . To probe this shift, we perform two-photon Raman spectroscopy on  $X(6, 0)$ , shown in Fig. 2(a). We initialize our molecules in either  $X(-1, 0)$  or  $X(-2, 0)$  via photoassociation [31] and use  $0_u^+(-4, 1)$  or  $0_u^+(-5, 1)$  as the intermediate state to maximize the two-photon transition rate. The choice of initial and intermediate states does not strongly affect the measured  $S$  since the lattice is far detuned from any resonances that would shift the binding energies of these

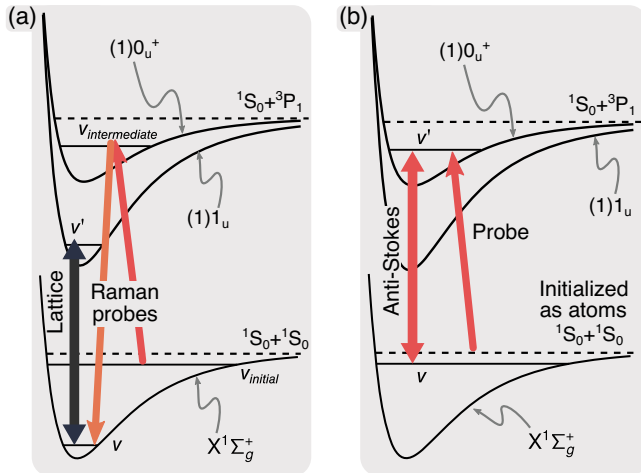


FIG. 1. Line strength measurement schemes for a pair of molecular vibrational states ( $v, v'$ ). (a) For deeply bound states of  $1_u$ , Raman spectroscopy was performed on  $X^1\Sigma_g^+$  molecules initialized in near-threshold vibrational states. (b) For weakly bound states of  $1_u$  and  $0_u^+$ , spectroscopic probing was performed on  $^1S_0$  atoms.

states. The Raman lasers are detuned from the intermediate state by 20 MHz, and the frequency of the first Raman leg is swept, while the second is kept fixed. Measurement of the two-photon resonance frequency at various  $\Delta$  gives the expected dispersive behavior, as shown in Fig. 2(b). Transition strengths are inextricably linked to polarizability, and in the Supplemental Material [31] we show that the

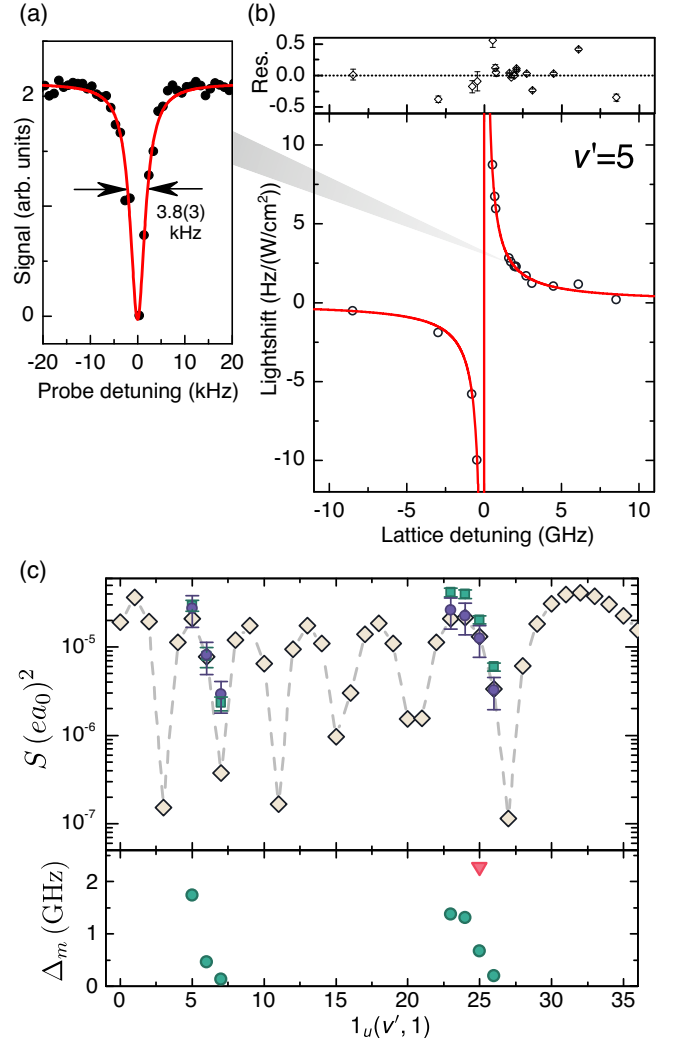


FIG. 2. (a) A two-photon Raman depletion line shape. For this trace, the differential light shift of the  $X$  states is nearly nulled, resulting in a narrow power-broadened linewidth of 3.8(3) kHz inferred from a Lorentzian fit. (b) The Raman peak locations (open circles) exhibit dispersive behavior as the lattice frequency is swept across the  $1_u$  state (shown here for  $v' = 5$ ). The solid red line is the fit to the avoided crossing of the form  $f_R^2/4\Delta$ . Residuals have units of  $\text{Hz}/(\text{W}/\text{cm}^2)$ . Error bars denote  $1\sigma$  uncertainties. (c) Line strengths of  $X(6, 0) \rightarrow 1_u(v', 1)$  (green circles, measured and calibrated to  $^1S_0$  Sr polarizability; purple squares, measured with intensity estimated from direct imaging of beam waist; yellow diamonds, calculated using the Morse potential). Also shown are the magic lattice detunings relative to the nearest  $1_u$  state for a given pair of  $X$  states [green circles,  $X(-1, 0) \rightarrow X(6, 0)$ ; red triangle,  $X(-1, 0) \rightarrow X(4, 0)$ ].

ratio of  $f_R$  to the axial trap frequency of  $X(-1,0)$  molecules implies that, away from any resonances, the baseline polarizability ratio of  $X(6,0)$  and  $X(-1,0)$  is 1.392(15) at 907.59 nm. This is then converted to absolute values of  $S$  for  $X(6,0) \rightarrow 1_u(v',1)$  by calibrating to the known polarizability of  $^1S_0$  atomic strontium.

Using this technique, we measure seven line strengths, where all the  $1_u$  states are below the minimum of the  $0_u^+$  potential. As illustrated in Fig. 2(c), experimentally  $S$  demonstrate decreasing trends in two ranges. Prior to this Letter, we used the binding energies calculated using the *ab initio* model of Ref. [32] to assign the vibrational quantum numbers  $v'$  in the ranges 1–3 and 19–22, where we find good agreement within 0.5% of the experimental binding energies (see Table SIII in the Supplemental Material [31]). To calculate the line strengths, we model  $X$  with a set of precise empirical potential parameters obtained from the hot pipe Fourier-transform spectroscopy [48] and use the *ab initio* electronic transition dipole moment. To our surprise, the calculated *ab initio* line strengths follow the opposite trends compared to the observations, and this persisted even when the electronic transition dipole moment was modified. This suggests that the  $v'$  assignment based on the *ab initio*  $1_u$  potential is erroneous. To overcome this, we take an alternative approach and model the short-range behavior of  $1_u$  with the simple Morse potential

$$V(R) = D_e[1 - e^{-\beta(R-R_e)}]^2 - D_e, \quad (3)$$

where  $D_e$  is the potential depth,  $R_e$  is the equilibrium bond length,  $\beta \equiv 2\pi\sqrt{2\mu\omega_e x_e c}/h$ , and  $\mu$  is the reduced mass of the dimer. In the presence of vibrational-rotational interaction, the energy levels are

$$E(v', J') = -D_e + \omega_e \left(v' + \frac{1}{2}\right) - \omega_e x_e \left(v' + \frac{1}{2}\right)^2 + \left[B_e - \alpha_e \left(v' + \frac{1}{2}\right)\right] J'(J' + 1), \quad (4)$$

where  $\omega_e$ ,  $x_e$ ,  $B_e$ , and  $\alpha_e$  are the vibrational, anharmonicity, rotational, and vibration-rotation coupling spectroscopic constants, respectively. As shown in the Supplemental Material [31], the best fit of the seven observed  $J' = 1$  levels to Eq. (4) indicates 15 vibrational states between the two groups and  $\omega_e x_e = 0.21150(28) \text{ cm}^{-1}$ . Rotational spectroscopy of  $J' = 3$  states yields  $\alpha_e = 7.068(11) \times 10^{-5} \text{ cm}^{-1}$ . The Morse eigenfunctions were obtained by numerically solving the nuclear Schrödinger equation on an adaptive grid [49]. As the classical turning points of the deeply bound  $X$  states are much further apart than those of  $1_u$ , the Frank-Condon factors for these transitions largely depend on the spatial variation of the ground-state nuclear wave function. Consequently, the

calculated  $S$  versus  $v'$  exhibit a characteristic interference-like pattern with  $v + 1$  maxima (this rule of thumb was observed to hold up to  $v \approx 12$ ). The measured experimental trends in  $S$  are well captured by the calculations only for  $v'$  assignments of 5–7 and 23–26 for the two ranges, as shown in Fig. 2(c) and Table SI (Supplemental Material [31]). The corresponding potential parameters are  $D_e = 6387.89(11) \text{ cm}^{-1}$  and  $R_e = 7.9027(5)a_0$ .

Hence, while the *ab initio* calculation has good accuracy in the long range, it underestimates  $D_e$  by approximately  $300 \text{ cm}^{-1}$  (5% relative difference). On the other hand, Eq. (3) allows for  $D_e$  to be empirically determined, but the simple potential cannot be extrapolated to the long range. To combine these complementary descriptions, we recast the *ab initio*  $1_u$  and  $0_u^+$  potentials in the Morse/Long-range (MLR) form [33,50] and fit to spectroscopic data, while fixing  $D_e$  and  $R_e$  to their empirical values found in this Letter. In the Supplemental Material [31], we provide details of the fitting process and the MLR parameters and recalculate the energy levels of  $0_u^+$  and  $1_u$  to benchmark against experimental values.

Turning to weakly bound states, an anti-Stokes laser selectively dresses  $X(v, J = 0)$  with a rovibrational state  $0_u^+(v', J' = 1)$  or  $1_u(v', J' = 1)$ , as shown in Fig. 1(b). Here, we perform spectroscopy on a trapped sample of ultracold atoms. Depletion occurs when a weak probe laser is on resonance with the dressed states

$$f_{\pm} = \frac{\Delta}{2} \pm \frac{\sqrt{f_R^2 + \Delta^2}}{2}, \quad (5)$$

where  $f_+$  ( $f_-$ ) is the resonance frequency of the blue-side (red-side) peak relative to the bare resonance ( $f_R = 0$ ), and  $\Delta$  is the coupling laser detuning. Figure 3(a) shows a sample trace when the anti-Stokes laser is slightly red-detuned from the  $X(-2,0) \rightarrow 0_u^+(-4,1)$  transition, revealing an Autler-Townes doublet. Although the atoms are tightly confined along the axial direction of the 1D lattice, the radial confinement is much weaker. At a finite temperature of a few microkelvin, the atoms occupy several motional states above the  $^1S_0 + ^1S_0$  continuum leading to an asymmetric line shape. We determined the location of the resonances by fitting to a doublet line shape function that accounts for these thermal effects [34].

Keeping the anti-Stokes laser intensity constant, the square of the doublet separation  $(f_+ - f_-)^2$  versus  $\Delta$  is a parabola whose minimum is  $f_R^2$ , as shown in Fig. 3(b). This presents an attractive method of determining line strengths, as opposed to measurements involving power broadening and transition rates, since frequency differences are robust against a wide variety of effects such as reference cavity drift, the overall trap-induced light shift, shot-to-shot signal fluctuations, and the fit line shape for the doublet. Moreover, by working strictly with transitions between  $J = 0$  and  $J' = 1$  and in the regime where the anti-Stokes

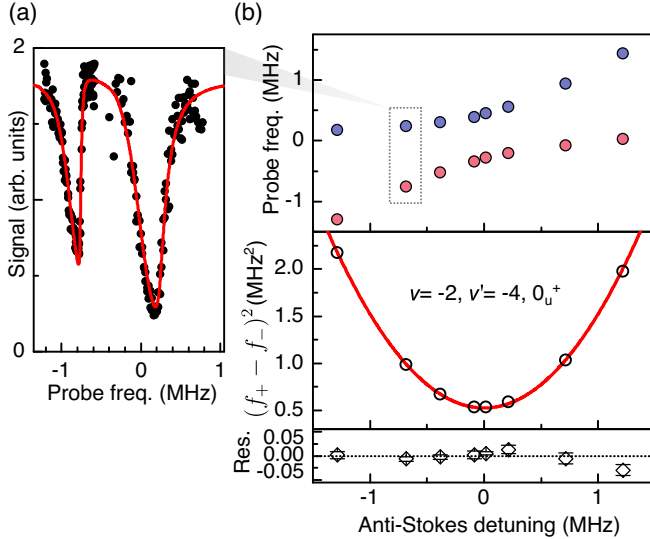


FIG. 3. (a) For a given detuning of the anti-Stokes laser from the bound-to-bound molecular transition, the probe is scanned to obtain an Autler-Townes doublet. (b) The locations of the blue-side peak (blue circles) and the red-side peak (red circles) form an avoided crossing. The square of the peak separations fit to a parabola (solid red) when plotted against the anti-Stokes detuning, the minimum of which is  $f_R^2$ . Error bars are propagated from  $1\sigma$  uncertainties in the peak locations from the line shape fit. Residuals are in units of MHz<sup>2</sup>.

detunings are larger than the Zeeman structure, the measured  $S$  are insensitive to laser polarization and are effectively between  $M = M' = 0$  states. The measured  $S$  and corresponding predictions from the *ab initio* [32] and MLR models are listed in Table I. For the weakly Coriolis-mixed states, both models perform similarly well. However, for the strongly Coriolis-mixed states, only the MLR model gives the correct  $0_u^+$  or  $1_u$  assignments and thus is more accurate in its predictions for  $S$ .

TABLE I. Measured (Expt.) line strengths for weakly bound  $0_u^+$  and  $1_u$  states from  $X$  for various vibrational pairs. Also shown for comparison are predictions from the *ab initio* (AI) and adjusted MLR potential constructed in this Letter. Starred values are strongly Coriolis-mixed states. Statistical uncertainties account for the  $1\sigma$  errors in the extracted Rabi frequencies as well as for laser power fluctuations. The units are  $10^{-3}(ea_0)^2$ .

$X(v, J = 0)$	State	$(v', J' = 1)$	AI	MLR	Expt.
-1	$0_u^+$	-4	3.09	2.77	2.57(4)
-2	$0_u^+$	-4	0.81	0.74	0.70(2)
-2	$0_u^+$	-5	5.86	5.06	4.30(6)
-3	$0_u^+$	-6	0.07*	8.89*	8.7(4)*
-1	$1_u$	-1	5.44	4.56	5.53(8)
-1	$1_u$	-2	0.36	0.33	0.40(1)
-2	$1_u$	-1	1.71	1.68	1.74(3)
-2	$1_u$	-2	6.95	5.82	8.0(1)
-3	$1_u$	-3	13.2*	2.46*	2.10(5)*

Our findings directly inform the engineering of favorable magic wavelength optical traps for a molecular clock, by means of elucidating the quantum chemistry of the strontium dimer. Just as in atomic lattice clocks, for a given baseline polarizability mismatch between the clock states, the required magic detuning  $\Delta_m$  (relative to a resonance between one of the clock states and an excited state) monotonically increases with the line strength [see Fig. 2(c) and Table SI [31]]. The sensitivity of the clock transition to lattice frequency inaccuracies is simply the slope of the lattice-induced light shift at the magic detuning,  $-f_R^2/4\Delta_m^2$ , and would decrease monotonically for larger  $S$  (and hence larger  $\Delta_m$ ). Therefore, magic wavelengths based on stronger transitions place less stringent constraints on the required frequency stability of the lattice laser and on the bandwidth of the spectral filter that suppresses the lattice laser noise away from the carrier (such as amplified spontaneous emission). To this end, we compute  $S$  between

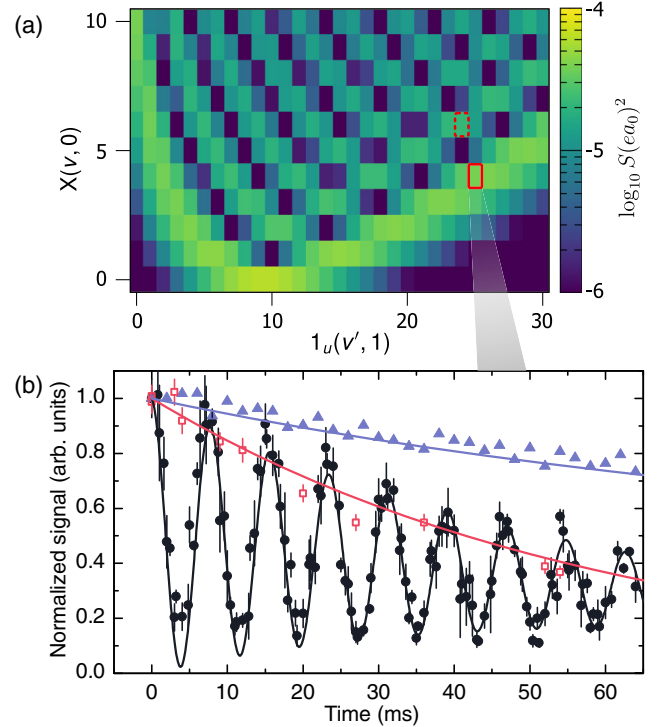


FIG. 4. (a) Line strengths of deeply bound states of  $1_u$  to  $X$ . Solid rectangle: the transition used for the magic wavelength in this Letter. Dashed rectangle: our previous work [21]. (b) Two-photon Rabi oscillations between  $X(-1, 0)$  and  $X(4, 0)$  (black circles). Here, favorable magic trapping is achieved by tuning the lattice near the  $X(4, 0) \rightarrow 1_u(25, 1)$  transition. Also shown are the normalized population decay of  $X(4, 0)$  (red squares) and  $X(-1, 0)$  (blue triangles). Black line: fit to  $A \exp(-t/T_1)[1 + \exp(-t/T_2^{\text{Rabi}}) \cos(\omega t - \phi)]$ . Red and blue lines are fits to the rate equation  $\dot{N} = -k_\gamma N^\gamma$  for the molecular number  $N$  with  $\gamma = 1$  and  $2$ , respectively, and  $k_\gamma$  as a free parameter. Error bars are  $1\sigma$  uncertainties.

the lower-lying  $J' = 1$  states of  $1_u$  and several deeply bound  $J = 0$  states of  $X$ , as shown in Fig. 4(a). For  $X(4, 0)$ , the state  $1_u(25, 1)$  has one of the largest predicted line strengths among several  $v'$  in the vicinity. The measured magic frequency at 330.302 750 449(104) THz corresponds to a detuning  $\Delta_m = 2.298(41)$  GHz from the  $X(4, 0) \rightarrow 1_u(25, 1)$  resonance and is the largest studied in this Letter. Operating the molecular clock at this magic wavelength, we demonstrate long-lived two-photon Rabi oscillations [ $T_2^{\text{Rabi}} = 77(6)$  ms,  $T_1 = 127(8)$  ms] between the clock states  $X(-1, 0)$  and  $X(4, 0)$ , as shown in Fig. 4(b) and described in the caption. This represents a significant improvement in coherent light-molecule interactions over our previous experiment [21]. The oscillations are predominantly damped by the loss of  $X(4, 0)$  molecules, which has a  $1/e$  lifetime of 60(2) ms at a trap depth of  $k_B \times 12(1)$   $\mu$ K. The single-body losses are faster for deeper traps, which indicates scattering of the lattice light. Here, analysis may be confounded by the linewidth of the lattice trap laser, since the deeply bound  $1_u$  states are expected to be much narrower ( $\Gamma_e \lesssim 2\pi \times 6$  kHz), and the situation is that of broadband scattering. Further investigations using the MLR potential curves can also help lend credence to specific loss mechanisms, such as multiphoton scattering, or to rule them out quantitatively.

In summary, we have measured the line strengths of several  $0_u^+$  and  $1_u$  states connecting to the ground-state  $X$  potential in two different regimes—weakly bound near-threshold states and deeply bound states—of ultracold lattice-trapped  $\text{Sr}_2$  molecules used in a molecular clock. The measurements were used to obtain analytic MLR potential curves for  $0_u^+$  and  $1_u$  that are in good agreement with previously published binding energies and those found in this Letter. In particular, we demonstrate the reliability of the constructed  $1_u$  potential by predicting and verifying states that have large transition strengths to  $X$ , which is an important criterion for the construction of magic optical traps. We presented an improved choice of a magic trap that led to a coherent control of the clock states for a record duration of nearly 100 ms. Furthermore, our accurate model will help elucidate the processes that contribute to the quenched molecular lifetimes and inform stimulated adiabatic pathways for ground-state preparation in future work, raising the prospects for a comprehensive vibrational spectroscopy of the ground potential as a high-precision test of molecular quantum electrodynamics and possible new physics.

We are grateful to A. Liberman and Y. Chai for contributions to the experiment. We acknowledge support from NSF Grant No. PHY-1911959 and ONR Grant No. N00014-17-1-2246. R. M. and I. M. also acknowledge the Polish National Science Center Grant No. 2016/20/W/ST4/00314.

\*Present address: Helmholtz-Institut Mainz, Johannes Gutenberg University, 55128 Mainz, Germany.

†Present address: Morgan Stanley, 1585 Broadway, New York, New York 10036, USA.

‡Present address: Atom Computing, Inc., 918 Parker Street, Berkeley, California 94710, USA.

§tanya.zelevinsky@columbia.edu

- [1] V. Andreev, D. G. Ang, D. DeMille, J. M. Doyle, G. Gabrielse, J. Haefner, N. R. Hutzler, Z. Lasner, C. Meisenhelder, B. R. O'Leary, C. D. Panda, A. D. West, E. P. West, X. Wu (A. C. M. E. Collaboration), Improved limit on the electric dipole moment of the electron, *Nature (London)* **562**, 355 (2018).
- [2] J. Lim, J. R. Almond, M. A. Trigatzis, J. A. Devlin, N. J. Fitch, B. E. Sauer, M. R. Tarbutt, and E. A. Hinds, Laser Cooled YbF Molecules for Measuring the Electrons Electric Dipole Moment, *Phys. Rev. Lett.* **120**, 123201 (2018).
- [3] I. Kozyryev and N. R. Hutzler, Precision Measurement of Time-Reversal Symmetry Violation with Laser-Cooled Polyatomic Molecules, *Phys. Rev. Lett.* **119**, 133002 (2017).
- [4] J. Kobayashi, A. Ogino, and S. Inouye, Measurement of the variation of electron-to-proton mass ratio using ultracold molecules produced from laser-cooled atoms, *Nat. Commun.* **10**, 3771 (2019).
- [5] R. Carollo, A. Frenett, and D. Hanneke, Two-photon vibrational transitions in  $^{16}\text{O}_2^+$  as probes of variation of the proton-to-electron mass ratio, *Atoms* **7**, 1 (2019).
- [6] M. Borkowski, A. A. Buchachenko, R. Ciuryo, P. S. Julienne, H. Yamada, Y. Kikuchi, Y. Takasu, and Y. Takahashi, Weakly bound molecules as sensors of new gravitylike forces, *Sci. Rep.* **9**, 14807 (2019).
- [7] R. V. Krems, Cold controlled chemistry, *Phys. Chem. Chem. Phys.* **10**, 4079 (2008).
- [8] N. Balakrishnan, Perspective: Ultracold molecules and the dawn of cold controlled chemistry, *J. Chem. Phys.* **145**, 150901 (2016).
- [9] J. L. Bohn, A. M. Rey, and J. Ye, Cold molecules: Progress in quantum engineering of chemistry and quantum matter, *Science* **357**, 1002 (2017).
- [10] M.-G. Hu, Y. Liu, D. D. Grimes, Y.-W. Lin, A. H. Gheorghe, R. Vexiau, N. Bouloufa-Maafa, O. Dulieu, T. Rosenband, and K.-K. Ni, Direct observation of bimolecular reactions of ultracold KRb molecules, *Science* **366**, 1111 (2019).
- [11] M. Guo, X. Ye, J. He, M. L. González-Martínez, R. Vexiau, G. Quémener, and D. Wang, Dipolar Collisions of Ultracold Ground-State Bosonic Molecules, *Phys. Rev. X* **8**, 041044 (2018).
- [12] M. McDonald, B. McGuyer, F. Apfelbeck, C.-H. Lee, I. Majewska, R. Moszynski, and T. Zelevinsky, Photodissociation of ultracold diatomic strontium molecules with quantum state control, *Nature (London)* **535**, 122 (2016).
- [13] J. A. Blackmore, L. Caldwell, P. D. Gregory, E. M. Bridge, R. Sawant, J. Aldegunde, J. Mur-Petit, D. Jaksch, J. M. Hutson, B. Sauer, M. R. Tarbutt, and S. L. Comish, Ultracold molecules for quantum simulation: Rotational coherences in CaF and RbCs, *Quantum Sci. Tech.* **4**, 014010 (2018).

- [14] E. Altman, K. R. Brown, G. Carleo, L. D. Carr, E. Demler, C. Chin, B. DeMarco, S. E. Economou, M. Eriksson, K.-M. C. Fu *et al.*, Quantum simulators: Architectures and opportunities, [arXiv:1912.06938](https://arxiv.org/abs/1912.06938).
- [15] A. Micheli, G. K. Brennen, and P. Zoller, A toolbox for lattice-spin models with polar molecules, *Nat. Phys.* **2**, 341 (2006).
- [16] K.-K. Ni, T. Rosenband, and D. D. Grimes, Dipolar exchange quantum logic gate with polar molecules, *Chem. Sci.* **9**, 6830 (2018).
- [17] E. R. Hudson and W. C. Campbell, Dipolar quantum logic for freely rotating trapped molecular ions, *Phys. Rev. A* **98**, 040302(R) (2018).
- [18] M. Hughes, M. D. Frye, R. Sawant, G. Bhole, J. A. Jones, S. L. Cornish, M. R. Tarbutt, J. M. Hutson, D. Jaksch, and J. Mur-Petit, Robust entangling gate for polar molecules using magnetic and microwave fields, *Phys. Rev. A* **101**, 062308 (2020).
- [19] P. Yu, L. W. Cheuk, I. Kozyryev, and J. M. Doyle, A scalable quantum computing platform using symmetric-top molecules, *New J. Phys.* **21**, 093049 (2019).
- [20] C. Wang, X. Yi, J. Mawdsley, M. Kim, Z. Wang, and R. Han, An on-chip fully electronic molecular clock based on sub-terahertz rotational spectroscopy, *National electronics review* **1**, 421 (2018).
- [21] S. S. Kondov, C.-H. Lee, K. H. Leung, C. Liedl, I. Majewska, R. Moszynski, and T. Zelevinsky, Molecular lattice clock with long vibrational coherence, *Nat. Phys.* **15**, 1118 (2019).
- [22] R. Bause, M. Li, A. Schindewolf, X.-Y. Chen, M. Duda, S. Kotochigova, I. Bloch, and X.-Y. Luo, Tune-Out and Magic Wavelengths for Ground-State  $^{23}\text{Na}^{40}\text{K}$  Molecules, *Phys. Rev. Lett.* **125**, 023201 (2020).
- [23] F. Seeßelberg, X.-Y. Luo, M. Li, R. Bause, S. Kotochigova, I. Bloch, and C. Gohle, Extending Rotational Coherence of Interacting Polar Molecules in a Spin-Decoupled Magic Trap, *Phys. Rev. Lett.* **121**, 253401 (2018).
- [24] R. B. Hutson, A. Goban, G. E. Marti, L. Sonderhouse, C. Sanner, and J. Ye, Engineering Quantum States of Matter for Atomic Clocks in Shallow Optical Lattices, *Phys. Rev. Lett.* **123**, 123401 (2019).
- [25] S. Dörscher, R. Schwarz, A. Al-Masoudi, S. Falke, U. Sterr, and C. Lisdat, Lattice-induced photon scattering in an optical lattice clock, *Phys. Rev. A* **97**, 063419 (2018).
- [26] J. W. Park, S. A. Will, and M. W. Zwierlein, Two-photon pathway to ultracold ground state molecules of  $^{23}\text{Na}^{40}\text{K}$ , *New J. Phys.* **17**, 075016 (2015).
- [27] M. Guo, R. Vexiau, B. Zhu, B. Lu, N. Bouloufa-Maafa, O. Dulieu, and D. Wang, High-resolution molecular spectroscopy for producing ultracold absolute-ground-state  $^{23}\text{Na}^{87}\text{Rb}$  molecules, *Phys. Rev. A* **96**, 052505 (2017).
- [28] K. Aikawa, D. Akamatsu, M. Hayashi, J. Kobayashi, M. Ueda, and S. Inouye, Predicting and verifying transition strengths from weakly bound molecules, *Phys. Rev. A* **83**, 042706 (2011).
- [29] A. Ciamei, A. Bayerle, C.-C. Chen, B. Pasquiou, and F. Schreck, Efficient production of long-lived ultracold  $\text{Sr}_2$  molecules, *Phys. Rev. A* **96**, 013406 (2017).
- [30] A. Hansson and J. K. Watson, A comment on Hnl-London factors, *J. Mol. Spectrosc.* **233**, 169 (2005).
- [31] See Supplemental Material at <http://link.aps.org/supplemental/10.1103/PhysRevLett.125.153001> for details on the experimental methods, determination of the spectroscopic constants, the best fit potential parameters of the Morse/Long-range potentials, and additional data, which includes Refs. [22,32–47].
- [32] W. Skomorowski, F. Pawowski, C. P. Koch, and R. Moszynski, Rovibrational dynamics of the strontium molecule in the  $A^1\Sigma_u^+$ ,  $c^3\Pi_u$ , and  $a^3\Sigma_u^+$  manifold from state-of-the-art *ab initio* calculations, *J. Chem. Phys.* **136**, 194306 (2012).
- [33] R. J. Le Roy, N. S. Dattani, J. A. Coxon, A. J. Ross, P. Crozet, and C. Linton, Accurate analytic potentials for  $\text{Li}_2(X^1\Sigma_g^+)$  and  $\text{Li}_2(A^1\Sigma_u^+)$  from 2 to 90 Å, and the radiative lifetime of  $\text{Li}(2p)$ , *J. Chem. Phys.* **131**, 204309 (2009).
- [34] B. McGuyer, M. McDonald, G. Z. Iwata, M. Tarallo, A. Grier, F. Apfelbeck, and T. Zelevinsky, High-precision spectroscopy of ultracold molecules in an optical lattice, *New J. Phys.* **17**, 055004 (2015).
- [35] G. Reinaudi, C. B. Osborn, M. McDonald, S. Kotochigova, and T. Zelevinsky, Optical Production of Stable Ultracold  $^{88}\text{Sr}_2$  Molecules, *Phys. Rev. Lett.* **109**, 115303 (2012).
- [36] J. Stenger, H. Schnatz, C. Tamm, and H. R. Telle, Ultra-precise Measurement of Optical Frequency Ratios, *Phys. Rev. Lett.* **88**, 073601 (2002).
- [37] N. Scharnhorst, J. B. Wübbena, S. Hannig, K. Jakobsen, J. Kramer, I. D. Leroux, and P. O. Schmidt, High-bandwidth transfer of phase stability through a fiber frequency comb, *Opt. Express* **23**, 19771 (2015).
- [38] M. McDonald, B. H. McGuyer, G. Z. Iwata, and T. Zelevinsky, Thermometry via Light Shifts in Optical Lattices, *Phys. Rev. Lett.* **114**, 023001 (2015).
- [39] B. H. McGuyer, M. McDonald, G. Z. Iwata, M. G. Tarallo, W. Skomorowski, R. Moszynski, and T. Zelevinsky, Precise study of asymptotic physics with subradiant ultracold molecules, *Nat. Phys.* **11**, 32 (2015).
- [40] S. G. Porsev, A. D. Ludlow, M. M. Boyd, and J. Ye, Determination of Sr properties for a high-accuracy optical clock, *Phys. Rev. A* **78**, 032508 (2008).
- [41] I. Ushijima, M. Takamoto, and H. Katori, Operational Magic Intensity for Sr Optical Lattice Clocks, *Phys. Rev. Lett.* **121**, 263202 (2018).
- [42] M. Borkowski, P. Morzyński, R. Ciuryło, P. S. Julienne, M. Yan, B. J. DeSalvo, and T. C. Killian, Mass scaling and nonadiabatic effects in photoassociation spectroscopy of ultracold strontium atoms, *Phys. Rev. A* **90**, 032713 (2014).
- [43] S. G. Porsev, M. S. Safronova, and C. W. Clark, Relativistic calculations of  $C_6$  and  $C_8$  coefficients for strontium dimers, *Phys. Rev. A* **90**, 052715 (2014).
- [44] J. Mitroy and J. Zhang, Dispersion and polarization interactions of the strontium atom, *Mol. Phys.* **108**, 1999 (2010).
- [45] G. Ferrari, P. Cancio, R. Drullinger, G. Giusfredi, N. Poli, M. Prevedelli, C. Toninelli, and G. M. Tino, Precision Frequency Measurement of Visible Intercombination Lines of Strontium, *Phys. Rev. Lett.* **91**, 243002 (2003).
- [46] M. McDonald, *High Precision Optical Spectroscopy and Quantum State Selected Photodissociation of Ultracold  $^{88}\text{Sr}_2$  Molecules in an Optical Lattice* (Springer, New York, 2017).

- [47] T. Zelevinsky, M. M. Boyd, A. D. Ludlow, T. Ido, J. Ye, R. Ciuryło, P. Naidon, and P. S. Julienne, Narrow Line Photoassociation in an Optical Lattice, *Phys. Rev. Lett.* **96**, 203201 (2006).
- [48] A. Stein, H. Knckel, and E. Tiemann, The  $^1S + ^1S$  asymptote of  $Sr_2$  studied by Fourier-transform spectroscopy, *Eur. Phys. J. D* **57**, 171 (2010).
- [49] E. Tiesinga, C. J. Williams, and P. S. Julienne, Photoassociative spectroscopy of highly excited vibrational levels of alkali-metal dimers: Green-function approach for eigenvalue solvers, *Phys. Rev. A* **57**, 4257 (1998).
- [50] R. J. Le Roy and R. D. Henderson, A new potential function form incorporating extended long-range behaviour: Application to ground-state  $Ca_2$ , *Mol. Phys.* **105**, 663 (2007).